International Journal of Gender, Science and Technology
ISSN: 2040-0748
UGC Care Group I Journal.
Vol-11 Issue-02 Dec 2022
https://ijgst.com.2022.v11.i2.pp20-24

Hexagonal Nanomagnets with Reversible Magnetization Capability

Dr.Krishnan Gopala[1], Professor[1], Department of ECE, Siddhartha Institute of Technology & Sciences,Telangana, India

Nalla Kumar Ajay[2], Assistant Professor[2], Department of CSE, Siddhartha Institute of Technology & Sciences,Telangana, India.

Abstract

Depending on the geometry and the magnetic material with its magneto crystalline anisotropy, magnetic nanostructures frequently display fascinating shape anisotropies that may provide novel potential applications. It is possible to investigate the impact of superposing shape anisotropies with various magneto crystalline anisotropies due to the roughly two-orders-of-magnitude difference in the anisotropy constants of the pure magnetic materials iron, cobalt, and nickel. In this article, we provide results from simulations of three distinct hexagonal-shaped nanomagnets made of iron, cobalt, and nickel that are angle-dependent. For nickel nanomagnets, the typical hysteresis loops, which are typically devoid of steps, are visible. However, cobalt produces a wide variety of magnetization reversal processes with several steps that change over the course of repeated simulations as a result of variations in the anisotropy axes in different grains of the nanoparticles. Iron provides the best compromise between steps along the hysteresis loops which were proven to be correlated with stable intermediate states, usable for quaternary or higher-order storage devices, and reliable magnetization reversal processes even for sputtered samples with arbitrary anisotropy orientations in the single grains. Our examinations reveal that for nanomagnets on dimensions of a few hundred nanometres, iron is the ideal material not only for new magnetic data storage applications, but also for basic investigations of new and possibly technologically usable magnetization reversal processes.

Introduction

Magnetic nanostructures are of high interest for basic research of the interplay between magneto crystalline and shape anisotropy [1] as well as for a broad range of applications from biomedicine to data storage systems [2]. Recently, often magnetic nanofibers were investigated, e.g., fibers with structured “nano traps” which enabled multiple magnetic states [3]. On the other hand, bent nanofibers offer interesting magnetization reversal processes [4, 5] and domain wall propagation modes [6, 7]. While single magnetic nanowires are often correlated with the racetrack memory, using domain wall propagateton for data storage and manipulation [8–10], the combination of two or more magnetic nanowires allows for creating quaternary and higher-order memory devices. This idea is similar to the intermediate resistance states recently found in Cu/cobalt ferrite/Pt sandwich strucktrue which could also be used for multilevel resistive switching [11]. Such open frames in square [12] or hexagonal shape [13] from iron (Fe) were shown to exhibit one or more steps along the slope of the hysteresis loop, often correlated with stable intermediate states which can be used as addictional data storage state, enabling storing two or more bits in one storage position. For other materials, such as nickel, stable intermediate states do not necessarily occur [14]. Closed square Fe nanodots did not reveal such stable intermediate states, either [15]. However, since closed areas are easier to produce lithographically than frames with thin “walls”, such nanoparticles would be of interEst for bit-patterned media and other applications if they also showed more than the common two magnetic states at vanishing external magnetic field. In addition, other magnetic materials may offer new magnetization riversale processes, such as triangular permalloy micropartclues which showed magnetization reversal either stepwise or via an intermediate state, depending on the particse orientation [16]. Cobalt, on the other hand, was found to exhibit different intermediate states for diverse shapes [17, 18]. Here we report on micromagnetic simulations of nanoparticles of three hexagonal shapes, modelled with nickel (Ni), iron and cobalt (Co) to span a broad range of magneto crystalline anisotropies, investigated in deependance of the in-plane angle of the external magnetic field. In this way, an overview can be given under which condictions the interplay between shape and material result in stable intermediate states which may be used for new storage devices.

Simulations

For the micromagnetic simulations described here, the micromagnetic simulation program Object Oriented Micryomagnetic Framework (OOMMF) was used [19]. For the materials under examination, the original OOMMF material parameters were adopted, corresponding to tipictal literature values [20–22]:

- Ni: $M_s = 490 \times 10^3$ A/m, $A = 9 \times 10^{-12}$ J/m, $K_1 = -5.7 \times 10^3$ J/m^3,
- Fe: $M_s = 1700 \times 10^3$ A/m, $A = 21 \times 10^{-12}$ J/m, $K_1 = 48 \times 10^3$ J/m^3,
- Co: $M_s = 1400 \times 10^3$ A/m, $A = 30 \times 10^{-12}$ J/m, $K_1 = 520 \times 10^3$ J/m^3,

where Ms is the magnetization at saturation, A is the exchange constant, and K1 is the magneto crystalline anisotropy constant. It should be mentioned that Ni and Fe have a cubic anisotropy

https://ijgst.com.2022.v11.i2.pp20-24

while Co shows a uniaxial anisotropy. The fundamental equation for simulation is the Landau–Lipschitz–Gilbert (LLG) consisting of the presessional and damping terms set at the temperature T = 0 K. The measure of the damping is represented by the phenomenological Gilbert constant. It should be mentioned that while the saturation magnetization Ms and the exchange constant A are of the same order of magnitude for all three materials, the anisotropy constint K1 is growing by approximately one order of magnature from Ni to Fe and from Fe to Co, suggesting a significantly reduced influence of the magneto crystalline anisotropy in Ni nanoparticles, as compared to Fe, while the magneto crystallineanisotropy should be clearly doominnating in the Co nanoparticles under investigation. The Gilbert damping constant α was set to 0.5 (quasistatic case), and the mesh size of the elementary cube was equal to d = 5 nm. To model sputtered systems without theremal after-treatment, random anisotropy axes were chopseen, in the meaning of random distribution of the axis orientations between cubes creating the meshed samples. Maximum simulated magnetic fields were chosen between 100 MT and 1 T, depending on the material, always endSuring that the saturation was reached, i.e., that mangetaxation reversal was completed. Sample orientations were varied between 0 ◦ and 90◦. As a result, longitudinal magnetization components ML and transverse magnetization components MT are given, referenced to the external magnetic field direction, as usual, with ML being parallel to the external magnetic field and MT being perpendicular to it. The three different shapes under examination are depicked in Fig. 1a–c. The thickness was always chosen as 5 nm. To make the three shapes comparable, their areas were calculated to be identical, resulting in the following lateral dimensions of the rectangle covering the figures: • equilateral: width 500 nm, height 500 nm • rectangular: width 360 nm, height 785 nm • concave: width 610 nm, height 530 nm

Results and discussion

Firstly, Fig. 2 depicts exemplary hysteresis loops (Longerundial and transverse) simulated for the equilateral hexagon prepared from nickel. While for the 0 ◦ Orienstation, the transverse magnetization MT shows a broad range in which it does not saturate, clearly broader than

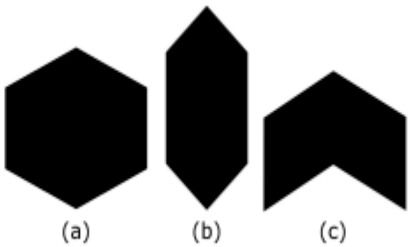

Fig. 1. Shapes used for the simulations in this paper (not drawn to scale): (a) equilateral, (b) rectangular, (c) concave

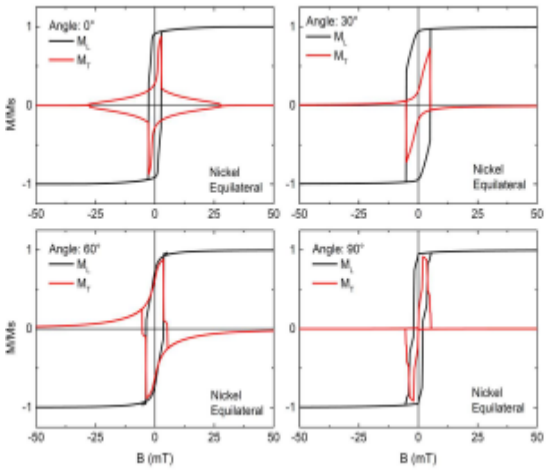

Fig. 2. Longitudinal (ML) and transversal hysteresis loops (MT), simulated for the equilateral hexagon prepared from nickel.

visible in ML, both values are similar for the other angels under examination. For 60◦ and 90◦ angles, steps are visible along the slope of the hysteresis loop which will be examined further below. Changing the material from nickel to iron, Fig. 3 shows broader hysteresis loops and more steps along the slopes of the hysteresis loops. In all angles besides 30◦,compareIng transversal and longitudinal hysteresis loops shows that magnetization reversal is not finished when the Longerundial loop seems to be closed, i.e., the external magnitic field necessary for saturation is much larger than the coercive fields. This is also the case for the equilateral hexagon prepared from cobalt, except for the 90◦ orientation (Fig. 4). Here, the hysteresis loops become even broader, as could be expected due to Co having the largest anisotropy constint. In addition, the angles of 60◦ and 90◦ show even more steps than the same shape prepared from Fe. Next, Fig. 5 depicts exemplary hysteresis loops, simelated for the rectangular shape prepared from nickel. While the 0 ◦ orientation shows a longitudinal hysteresis curve

https://ijgst.com.2022.v11.i2.pp20-24

which is nearly closed and could be ministerprated as superparamagnetic, the transversal curve shows clearly a coherent rotation of the whole magnetization,

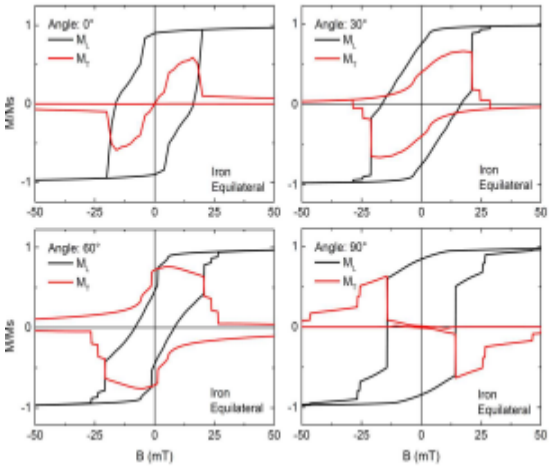

Fig. 3. Longitudinal and transverse hysteresis loops, simulated for the equilateral hexagon prepared from iron.

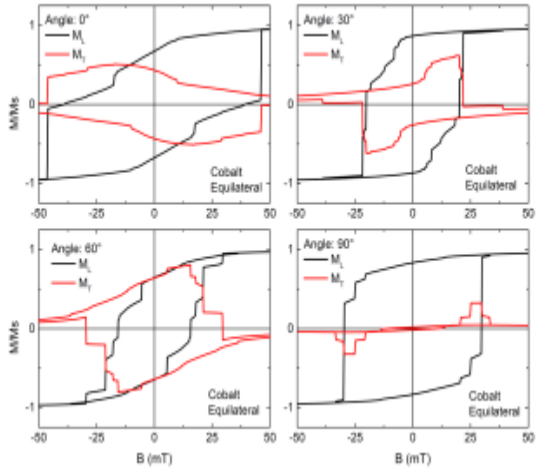

Fig. 4. Longitudinal and transversal hysteresis loops, simulated for the equilateral hexagon prepared from cobalt.

with the maximum values reaching 1, i.e., around vanfishing external magnetic field, the magnetization is compolitely oriented perpendicular to the field. The same evefact is visible for 30◦, while the maximum magnetization is slightly smaller for the 60◦ orientation and nearly vanashes for 90◦, indicating that here domain wall processes play a significant role. For iron, the rectangular hexagon again shows sevaearl steps along the hysteresis loops, for 0 ◦ again combinned with the effect that the longitudinal loop seems to be closed at smaller external magnetic fields than the transversal one (Fig. 6). For cobalt, again even more steps are visible in all angular orientations, as presented in Fig. 7. It should be mentioned that some of them are too small to be of techno logical relevance since for such nanomagnets, it is always necessary to take into account small deviations of

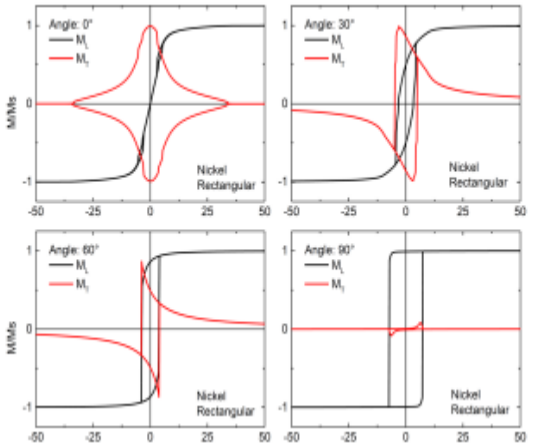

Fig. 5. Longitudinal and transversal hysteresis loops, simulated for the rectangular hexagon prepared from nickel.

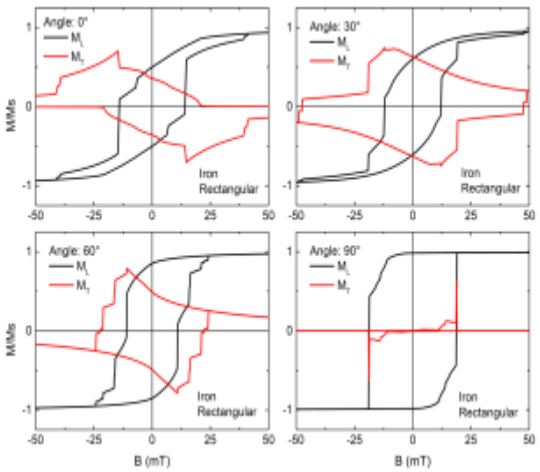

Fig. 6. Longitudinal and transversal hysteresis loops, simulated for the rectangular hexagon prepared from iron.

the shape due to the lithography process. This indicates that stopping and reversing the external magnetic field at a certain step is only possible if this step is broad enough; else the different states at remanence may be inseparable. In addition, it must be tested whether these states are not only stable at remanence, but can also be distinguished in a measurement. For the concave hexagon, the simulations of nickel again show clear broad transverse peaks and correspondIng steps in the hysteresis loops for all angles but 0 ◦ (Fig. 8), indicating the possibility to use these steps for quaternary data storage applications. For iron, Fig.

https://ijgst.com.2022.v11.i2.pp20-24

9 shows unusual longitudinal and transversal hysteresis loops, but not with significantly increased numbers of steps, indicating that this shape may be not favourable in comparison with both other nanoparticle shapes.

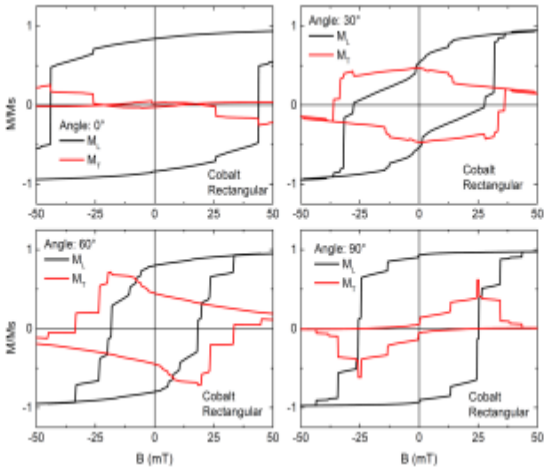

Fig. 7. Longitudinal and transversal hysteresis loops, simulated for the rectangular hexagon prepared from cobalt.

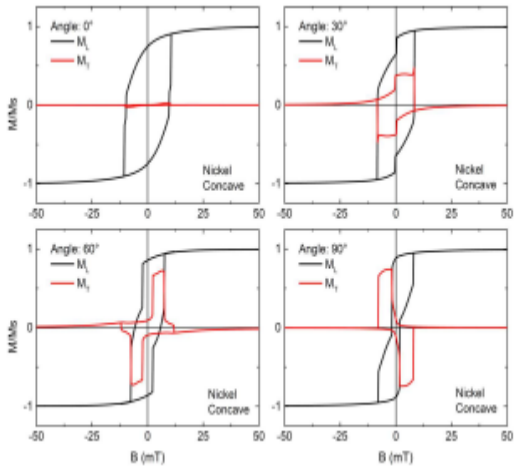

Fig. 8. Longitudinal and transversal hysteresis loops, simulated for the concave hexagon prepared from nickel. Finally, the concave hexagon prepared from Co (Fig. 10) depicts several steps in the longitudinal and the transverse hysteresis loops, offering several potentially stable states at remanence especially for the angles of 30◦ and 60◦. To visualize the differences between the three materials, Fig. 11 shows exemplary magnetization reversal processes of the rectangular hexagon under a field orientation of 90◦. For nickel, only a small deviation from the orientation of the external magnetic field ("vertical") is visible before magnetization is reversed. For iron, this effect is much stronger pronounced. Here, the final state before complete magnetization reversal shows a strong meander, comparable to the horseshoe state which can occur in open square frames and similar nano shapes. Cobalt, on the other hand, behaves differently. Even in the saturated case (left image), it is clearly visible that

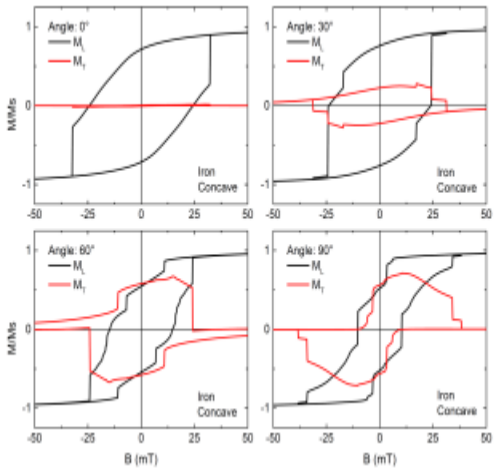

Fig. 9. Longitudinal and transversal hysteresis loops, simulated for the concave hexagon prepared from iron.

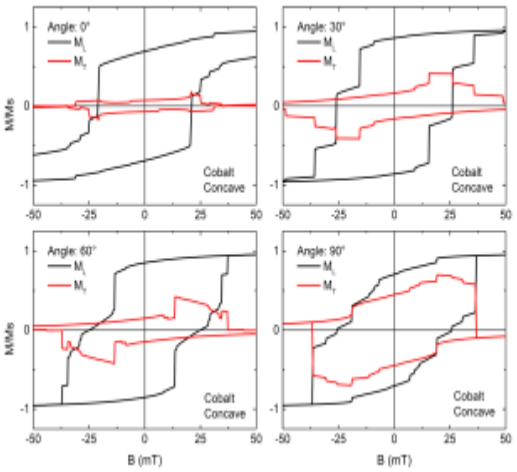

Fig. 10. Longitudinal and transversal hysteresis loops, simulated for the concave hexagon prepared from cobalt. the magnetization orientation differs in several small areas, arbitrarily distributed along the nanomagnet. With reduced external magnetic field, some of these regions — which are not clearly separated by domain walls — become more dominant and integrate other, sometimes smaller areas. Before the main step of the magnetization reversal occurs (from image 3 to image 4), there are also meander structures visible, but less structured than for the Fe nanomagnet. It should be mentioned that here still small areas are visible with the magnetization orientation differing from the surrounding material. Magnetization reversal thus

https://ijgst.com.2022.v11.i2.pp20-24

does not occur at once, as for iron or nickel, but in several steps, as visible in the 4th image in which most of the magnetization is switched, but several areas are still oriented against the external magnetic field which is now oriented from top to bottom. In the last image depicted here, magnetization reversal is still not completed; at the bottom corner a small area still has to switch.

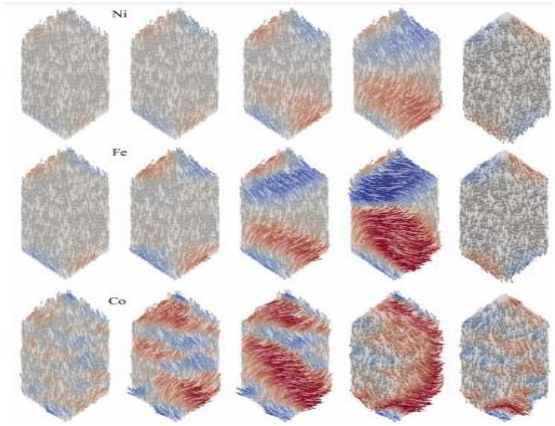

Fig. 11. Snapshots of key points of the magnetization reversal processes for Ni, Fe, and Co in the rectangular hexagon for the external magnetic field oriented along 90◦. Magnetization orientation sweeping from "up" to "down" (see inset at the top). Color code: red — magnetization pointing to the right, blue — magnetization pointing to the left. The full videos are available as supplementary material.

These images indicate that Co is not the ideal material for nanostructures in the dimensions examined here. The most interesting material for these dimensions seems to be iron, while for thinner structures, cobalt can be expected to show sufficiently high magneto crystalline anisotropy for an adequate interaction with the shape anisotropy, as it is the case here for iron.

Conclusion

By using micromagnetic simulations, several hexagonal nanomagnets made of nickel, iron, and cobalt were examined. While cobalt's strong magneto crystalline anisotropy prevented reliable magnetization reversal processes for sputtered samples, or nanomagnets with arbitrary orientations of the single magnetic cells, nickel nanoparticles demonstrated straightforward magnetization reversal processes that were frequently based on coherent rotation of the magnetization. Iron demonstrated most promising numbers of stable intermediate states that could be clearly separated from one another for the sample size examined here in the range of about 100 nanometres. This makes especially the equilateral iron hexagon an interesting nanoparticle for the development of quaternary or higher order data storage devices

References

[1] H.J. Li, Q. Wu, M. Yue, Y. Peng, Y.Q. Li, J.M. Liang, D.J. Wang, J.X. Zhang, J. Magna. Magna. Mater. 481, 104 (2019).

[2] M. Tadic, S. Krall, Y. Lala tonne, L. Motte, Appl. Surf. Sci. 476, 641 (2019).

[3] C.C. Faulkner, M.D. Cooke, D.A. Allwood, D. Petit, D. Atkinson, R.P. Cowbarn, J. Appl. Phys. 95, 6717 (2004).

[4] P. Kern, C. Dope, T. Laconic, P. Stapinski, A. Hermann, J. Magn. Magn. Mater. 484, 37 (2019).

[5] T. Blachowicz, A. Ehrmann, J. Appl. Phys. 124, 152112 (2018).

[6] C. Garg, S.-H. Yang, T. Phung, A. Pushp, S.S.P. Parkin, Sci. Adv. 3, e1602804 (2017).

[7] R. Moreno, V.L. Carvalho-Santos, A.P. Espejo, D. Laroze, O. Chubykalo-Fesenko, D. Altbir, Phys. Rev. B 96, 184401 (2017).

[8] J. Grollier, P. Boullenc, V. Cros, A. Hamzic, A. Vaurès, A. Fert, G. Faini, Appl. Phys. Lett. 83, 509 (2003).

[9] N. Vernier, D.A. Allwood, D. Atkinson, M.D. Cooke, R.P. Cowburn, Europhys. Lett. 65, 526 (2004).

[10] S.-H. Yang, K.-S. Ryu, S.S.P. Parkin, Nat. Nanotechnol. 10, 221 (2015).

[11] S. Munjal, N. Khare, Appl. Phys. Lett. 113, 243501 (2018).

[12] T. Blachowicz, A. Ehrmann, J. Appl. Phys. 110, 073911 (2011). [13] T. Blachowicz, A. Ehrmann, J. Magn. Magn. Mater. 331, 21 (2013).

[14] R. Hertel, J. Appl. Phys. 90, 5752 (2001).

[15] A. Ehrmann, T. Blachowicz, Hyperfine Interact. 239, 8 (2018).

[16] D.A. Bizyaev, A.A. Bukharaev, A.P. Chuklanov, N.I. Nurgazizov, Phys. Solid State 60, 2194 (2018).

[17] F.J. Castano, C.A. Ross, A. Eilez, J. Phys. D Appl. Phys. 36, 2031 (2003).

[18] A. Ehrmann, T. Blachowicz, AIP Adv. 5, 097109 (2015).

[19] M.J. Donahue, D.G. Porter, OOMMF User's Guide, Version 1.0 Interagency Report NISTIR 6376, National Institute of Standards and Technology, Gaithersburg 1999.

[20] S. Michea, J. Briones, J.L. Palma, R. Lavín, J. Escrig, R. Rodríguez-Suárez, J.C. Denardin, J. Phys. D Appl. Phys. 47, 335001 (2014).

[21] E.F. Kneller, R. Hawig, IEEE Trans. Magn. 27, 3588 (1991).

[22] I.Z. Rahman, A. Boboc, K.M. Razeeb, M.A. Rahman, J. Magn. Magn. Mater. 290–291, 246 (2005). [23] A. Tillmanns, S. Oertker, B. Beschoten, G. Güntherodt, C. Leighton, I.K. Schuller, J. Nogués, Appl. Phys. Lett. 89, 202512 (2006).